

Effective Non-Local Reaction Kinetics for Transport in Physically and Chemically Heterogeneous Media

Marco Dentz

Institute of Environmental Assessment and Water Research (IDÆA-CSIC), Barcelona, Spain

Philippe Gouze

Géoscience, Université de Montpellier 2, CNRS, Montpellier, France

Jesus Carrera

Institute of Environmental Assessment and Water Research (IDÆA-CSIC), Barcelona, Spain

Abstract

The correct characterization of the effective reactive transport dynamics is an important issue for modeling reactive transport on the Darcy scale, specifically in situations in which reactions are localized, that is when different reactions occur in different portions of the porous medium. Under such conditions the conventional approach of homogenizing only the porous medium chemistry is not appropriate. We consider here reactive transport in a porous medium that is characterized by mass transfer between a mobile and a distribution of immobile regions. Chemical and physical heterogeneity are reflected by distributions of kinetic reaction rate constants and residence times in the immobile zones. We derive an effective reactive transport equation for the mobile solute that is characterized by non-local physical mass transfer and reaction terms. Specifically, chemical heterogeneity is upscaled

in terms of a reactive memory function that integrates both chemical and physical heterogeneity. Mass transfer limitations due to physical heterogeneity yield effective kinetic rate coefficients that can be much smaller than the volumetric average of the local scale coefficients. These results help to explain and quantify the often reported discrepancy between observed field reaction rate constants and the ones obtained under well mixed laboratory conditions. Furthermore, these results indicate that transport under physical and chemical heterogeneity cannot be upscaled separately.

1. Introduction

Modeling the fate of chemical species that react with rock-forming minerals is important for predicting situations related to water quality, risk assessment, subsurface storage or CO₂ sequestration performance, hydrocarbon production, etc. These processes are modeled from laboratory to catchment and reservoir scales. Yet, modeling is often performed in the frame of the single continuum approach where the scale dependence of fluid-mineral reactions inherits from that of flow and transport. While the theoretical basis for the definition of a pertinent support volume in the frame of the continuum approach have been investigated (e.g., Whitaker, 1999; Hornung, 1997), the underlying assumption that solute species are fully mixed and have access to all reactive surfaces of the rock-forming minerals is unrealistic. This is especially relevant in the case of chemically heterogeneous media over support volumes ranging from millimeters to several meters. Our work is motivated by the view that geological materials are heterogeneous and display both

chemical and physical heterogeneities that may display distinct scale dependence.

Permeability and diffusivity fields control water flow and conservative transport. The spatial distribution of reactive surface areas controls dissolution-precipitation rates. At the Darcy scale, all these parameters are related to porosity, but not only. For instance, diffusion path tortuosity and surface roughness affect diffusion and reactions, respectively. Whereas indirect measurements of these parameters can be performed to evaluate Darcy scale effective values, they can only be fully (i.e. geometrically) characterized at micro-scale. Similarly, the distribution of micro-porosity in the matrix (with pores often smaller than few microns) cannot be measured directly. The X-ray microtomography cross sections shown in Figure 1 display a typical example of reservoir rocks, with multi-scale grain size and matrix micro-porosity heterogeneity. This figure illustrates the expected complexity of the mass transfers between the macro-porosity (where fluid flow dominates) and the diffusion clusters displaying heterogeneous porosity.

Accounting for both chemical and physical heterogeneity, while keeping the computational advantages of the (single) continuum approach is essential for the development of practical (for instance, easily parameterizable using measurable data) and reliable modeling tools. It follows that upscaling of both chemical and physical heterogeneity is required. Along this line, pore-scale models have been used to investigate the effect of the spatial distribution of reaction rates (e.g., Li et al., 2006, 2007). Results point out that important discrepancies may occur between rates computed by continuum

models and pore-scale models depending on the chemical and physical heterogeneity of rock. Yet, it is difficult to separate the specific control of the chemical and physical heterogeneity and to derive general rules for upscaling processes. Conversely, several studies have considered the upscaling of mass transfer processes in heterogeneous media (e.g., Edwards et al., 1993; Quintard and Whitaker, 1994; Lichtner and Tartakovsky, 2003; Meile and Tuncay, 2006; Lichtner and Kang, 2007) using different analytical methods. However, physical and chemical mechanisms have often been investigated separately. Still, what emerges from these works is that small scale concentration gradients are not negligible when large scale heterogeneities are considered (e.g., Battiato et al., 2009) and a non-local description of the upscaled concentration is required (e.g., Hu et al., 1997; Espinoza and Valocchi, 1997; Kechagia et al., 2002; Lichtner and Kang, 2007; Liu et al., 2008; Donado et al., 2009).

Non-local approaches have been successfully applied for modeling the transport of inert tracers in heterogeneous media displaying non-Fickian behavior (e.g., Berkowitz et al., 2002; Dentz and Berkowitz, 2003; Schumer et al., 2003). Specifically, mass exchange between a distribution of regions where the fluid is immobile and the flowing region can be accounted for by non-local in-time formulations such as the multirate mass transfer (MRMT) model (e.g., Haggerty and Gorelick, 1995; Carrera et al., 1998; Haggerty et al., 2000). In the frame of the continuum approach, mobile and immobile domains coexist locally at the Darcy scale. Alternatively, multicontinuum models can be considered that account for multiple mobile and immobile continua (e.g., Lichtner and Kang, 2007). Obviously, the MRMT model is

well adapted to represent macroscale transport in fractured media, where the mobile region plays the role of fractures and the immobile regions represent matrix blocks (e.g., Neretnieks, 1980; Tsang et al., 1996). Nevertheless, several studies show that the MRMT approach is well suited to describe solute transport in different types of heterogeneous porous media, such as those where a sizeable fraction of the porosity is formed of dead end structures and low permeability zones or where hydraulic heterogeneity leads to travel time distributions analogous to those of diffusion into physically immobile regions (e.g., Haggerty and Gorelick, 1995; Carrera et al., 1998; Haggerty et al., 2000; Salamon et al., 2007; Gouze et al., 2008; Willmann et al., 2008; Silva et al., 2009). In fact, Willmann et al. (2010) reproduced the overall precipitation of mixing driven (fast) reactions through hydraulically heterogeneous porous media using a MRMT formulation. That is, non-local in time formulations can be used to represent both diffusion into immobile regions and the effect of heterogeneity in hydraulic conductivity.

The transport equation for a non-reactive dissolved species in a medium consisting of a mobile continuum and multiple immobile continua can be written as

$$\phi_m \frac{\partial c_m(\mathbf{x}, t)}{\partial t} + \nabla \cdot [\mathbf{q}(\mathbf{x}) - \mathbf{D}_m \nabla] c_m(\mathbf{x}, t) = j_B(\mathbf{x}, t), \quad (1a)$$

where $c_m(\mathbf{x}, t)$ is the species concentration (averaged over the support volume associated with position \mathbf{x}) in the mobile domain, \mathbf{D}_m is the bulk dispersion tensor, $\mathbf{q}(\mathbf{x})$ the Darcy velocity referring to the bulk volume. The porosity of the mobile domain ϕ_m denotes the ratio of the mobile pore volume to the bulk

volume. It is the product of the intrinsic mobile porosity with the mobile volume fraction. The mass exchange between the mobile continuum and the immobile continua is modeled by the source term $j_B(\mathbf{x}, t)$. The immobile regions are marked by a continuous variable α . The ensemble of immobile regions then is characterized statistically by the distribution density $\mathcal{P}(\alpha)$. The exchange term $j_B(\mathbf{x}, t)$ now can be written as the weighted sum over the exchange terms $j_B(\mathbf{x}, t|\alpha)$ between the mobile continuum and the immobile continua

$$j_B(\mathbf{x}, t) = \int_0^{\infty} d\alpha \mathcal{P}(\alpha) j_B(\mathbf{x}, t|\alpha). \quad (1b)$$

Mass balance in the immobile region of type α is thus expressed as

$$\phi_{im}(\alpha) \frac{\partial c_{im}(\mathbf{x}, t|\alpha)}{\partial t} = -j_B(\mathbf{x}, t|\alpha), \quad (1c)$$

where $c_{im}(\mathbf{x}, t|\alpha)$ and $\phi_{im}(\alpha)$ are the concentration and porosity in the immobile zone. As for the mobile porosity, the immobile porosity is referred to the bulk volume. The local exchange terms $j_B(\mathbf{x}, t|\alpha)$ are determined by the specific mass transfer mechanisms. For linear mass transfer processes, that is, processes that can be assimilated to diffusive and first-order kinetic mass transfer, the concentration in the immobile domain is a linear functional of the mobile concentration history, $C_m(x, t)$. Different forms can be adopted for this functional, but they can all be represented as the convolution of this history and a memory function $\varphi(t/\alpha)$ that characterizes the mass transfer process under consideration, as well as the geometry (including the mobile-immobile interface area) of the immobile zone of type α (e.g., Carrera et al., 1998; Haggerty et al., 2000). This memory function can be viewed as the

rate of change in immobile concentration, caused by a unit change in mobile concentration at time $t = 0$. Therefore,

$$c_{im}(\mathbf{x}, t|\alpha) = \int_0^t dt' \varphi(t - t'|\alpha) c_m(\mathbf{x}, t'), \quad (1d)$$

When different immobile regions overlap, the global mass exchange is simply the sum of the exchange rates with each of them. Therefore, a global memory function can be defined as

$$\varphi(t) = \int_0^\infty d\alpha \mathcal{P}(\alpha) \varphi(t|\alpha). \quad (1e)$$

The effective model (1) can be obtained by volume averaging (e.g., Whitaker, 1999) of a 'discrete' model that distinguishes explicitly between mobile and stagnant regions (e.g., Lichtner and Kang, 2007). The mobile and immobile concentrations $c_m(\mathbf{x}, t)$ and $c_{im}(\mathbf{x}, t)$ are averages over the mobile and stagnant regions, respectively. In this sense, the upscaling step from the discrete to the continuum model is integrated in the memory function, which contains information about shape and details of the stagnant regions. In fact, the model (1) accounts for physical heterogeneity of the medium at two levels. First the model acknowledges the presence of advection-dominated and diffusion-dominated domains (mesoscale heterogeneity) and second, it acknowledges the microscale heterogeneity of the immobile domains. This has been studied experimentally and theoretically by Gouze et al. (2008).

If the solute is reacting with rock-forming minerals, dissolution-precipitation reactions are expected both in the mobile and the immobile domains. The

general formulation for reactions with a mineral M is



where S_i denotes the dissolved species i and the ν_i are the stoichiometric coefficients. Kinetic reaction rates are governed by rate laws often based on transition state theory (e.g., Aagaard and Helgeson, 1982). In the absence of catalytic mechanisms, the reaction rate r ($r > 0$ denotes precipitation of mineral M) in any domain is written

$$r = -\vartheta\sigma \left(1 - \frac{\prod_i (\gamma_i c_i)^{\nu_i}}{K} \right), \quad (3)$$

where K is the equilibrium constant for the reaction, ϑ is the kinetic rate constant, γ_i is the activity coefficient for the i^{th} species with concentration c_i (either in the mobile or in the immobile domain) and σ is the specific reactive surface area defined as the accessible fluid-mineral area for the reactions per unit volume of rock. For dilute systems (i.e. low salinity fluids), $\gamma_i = 1$. Whereas the kinetic rate constants are usually known from laboratory measurements, the reactive surface area is the quantity with the greatest uncertainty. In fact, it is well-known (e.g., Steefel et al., 2005; Li et al., 2008) that field effective surface areas can be orders of magnitude smaller than those derived from actual measurements. Such discrepancy reflects, first, that access to reaction sites can be greatly delayed with respect to the arrival of reactants to the mobile zone. Second, it also reflects that reactive surface depends mainly on parameters that generally cannot be measured, such as the mineral surface morphology and the pore geometry, because of the

inherent heterogeneity of natural rocks. As a consequence, the heterogeneity of the reaction rate is mainly triggered by the heterogeneity of the specific reactive surface area. These effects can be captured by a transport model defined by Equations (1a) through (1d) that accounts for chemical reactions in the mobile and immobile regions (e.g., Lichtner and Kang, 2007; Liu et al., 2008; Donado et al., 2009). Here we adopt this approach. Another model that accounts for non-homogeneous physical and chemical medium properties on the field scale is the stochastic-convective streamtube approach (e.g., Ginn, 2001; Cirpka and Kitanidis, 2000; Seeboonruang and Ginn, 2006).

The objective of this paper is to study the combined control of physical and chemical heterogeneities on the extension and rate of dissolution (or precipitation). We focus on chemical systems far from the thermodynamic equilibrium where mass transfers are limited by kinetics. We adopt the multicontinuum reactive transport description presented in Lichtner and Kang (2007). In this framework reactions are defined separately for each immobile zone. Based on this approach, we derive in Section 2 an effective reactive transport equation for a single reactive solute species that is characterized by a non-local retardation term and a non-local reaction term. In Section 3, we investigate in detail the reaction behavior for the two end-member situations: (1) chemically homogeneous (i.e. same reaction rate) system with a distribution of transfer rate in the immobile domain and (2) homogeneous transport properties in the immobile domain with chemical heterogeneity (distribution of reaction rate in the immobile domain). Section 4 studies the behavior of effective reaction and transport coefficients. Conclusions are

drawn in Section 5.

2. Reactive Transport and Mass Transfer

We consider the problem of dissolution/precipitation in a multicontinuum medium characterized by a mobile and an ensemble of immobile regions, which communicate by linear mass transfer, as described by Equations (1a)–(1d). The immobile domains are characterized by the distribution of chemical and physical properties, more specifically, of kinetic rate coefficients and residence times. The dissolution reactions are described by the simplest form of (2)



In this case, the local reaction rate (3) can often be simplified to $r = k(c - c^{eq})$, where expressions for the kinetic rate constant k are discussed in Appendix A.

Reactive transport in the mobile domain is described by

$$\phi_m \frac{\partial c_m(\mathbf{x}, t)}{\partial t} + \nabla \cdot [\mathbf{q}(\mathbf{x}) - \mathbf{D}_m \nabla] c_m(\mathbf{x}, t) = -\phi_m k_m [c_m(\mathbf{x}, t) - c^{eq}] + j_B(\mathbf{x}, t). \quad (5)$$

Note that the porosity is referred to the total bulk volume. That is, it is given by $\phi_m = \phi'_m \chi_m$, where χ_m denotes the mobile volume fraction and ϕ'_m is the intrinsic porosity of the mobile domain, referred to the mobile bulk volume. We define here the rate coefficient as $k_m = k'_m / \phi'_m$ with k'_m the rate coefficient referred to the mobile bulk volume. Thus, k_m refers to the mobile pore volume, see also the discussion in Lichtner and Kang (2007).

As outlined in the Introduction, the type of medium we focus at is characterized macroscopically by a mobile region and a continuum of immobile regions, which are defined at each point in space. For such a macroscopic description to be valid, the support volume has to be large enough to be representative of the microscale heterogeneity. The immobile regions are marked by a continuous variable α . The distribution density of immobile zones is given by $\mathcal{P}(\alpha)$. The immobile porosity, reaction rate constant in the immobile domain $\Omega(\alpha)$ are denoted by $\phi_{im}(\alpha)$, and $k_{im}(\alpha)$. The inverse reaction rate constant $1/k_{im}(\alpha)$ defines the reaction time $\tau_r(\alpha)$. Figure 2 illustrates the conceptual model underlying the multicontinuum approach.

The average concentration distribution $c_{im}(\mathbf{x}, t|\alpha)$ in the immobile zone of type α satisfies the reaction equation

$$\phi_{im}(\alpha) \frac{\partial c_{im}(\mathbf{x}, t|\alpha)}{\partial t} = -\phi_{im}(\alpha) k_{im}(\alpha) [c_{im}(\mathbf{x}, t|\alpha) - c^{eq}] - j_B(\mathbf{x}, t|\alpha) \quad (6)$$

with the initial conditions

$$c_{im}(\mathbf{x}, t = 0|\alpha) = c^{eq}. \quad (7)$$

The immobile porosity of the immobile zone of type α referring to the bulk volume is $\phi_{im}(\alpha)$, and its volume fraction is denoted by $\chi_{im}(\alpha)$. Note that the immobile porosity $\phi_{im}(\alpha) = \phi'_{im}(\alpha)\chi_{im}(\alpha)$ with $\phi'_{im}(\alpha)$ the intrinsic porosity of the immobile zones. As above, the reaction rate constant here is referred to the immobile pore volume, $k_{im}(\alpha) = k'_{im}(\alpha)/\phi'_{im}(\alpha)$ with $k'_{im}(\alpha)$ the rate constant referred to the immobile bulk volume.

The mass exchange between the mobile and immobile regions is described by the local source term (1c). Using (1b) and (6), Eq. (5) for the mobile

concentration can be written as

$$\begin{aligned} \phi_m \frac{\partial c_m(\mathbf{x}, t)}{\partial t} + \nabla \cdot [\mathbf{q}(\mathbf{x}) - \mathbf{D}_m \nabla] c_m(\mathbf{x}, t) = -\phi_m k_m [c_m(\mathbf{x}, t) - c^{eq}] \\ - \int_0^\infty d\alpha \mathcal{P}(\alpha) \phi_{im}(\alpha) \left\{ \frac{\partial}{\partial t} c_{im}(\mathbf{x}, t|\alpha) + k_{im}(\alpha) [c_{im}(\mathbf{x}, t|\alpha) - c^{eq}] \right\}. \end{aligned} \quad (8)$$

Expressions for the local $j_B(\mathbf{x}, t|\alpha)$ are discussed below for matrix diffusion (i.e., for the case where physical heterogeneity can be described by the superposition of bodies where mass transfer is modeled by a diffusion equation) and first order terms, which can be used to approximate any memory function. Note that equations (6) and (8) are not closed for the mobile concentration. The closure of the system requires the specification of the mass transfer terms $j_B(\mathbf{x}, t|\alpha)$, that is, specification of the mass transfer mechanisms. In the following, we briefly review diffusive and first-order mass transfer mechanisms (e.g., Maloszewski and Zuber, 1985; Villermaux, 1987; Brusseau et al., 1989; Valocchi, 1990; Sardin et al., 1991; Haggerty and Gorelick, 1995; Carrera et al., 1998; Haggerty et al., 2000).

2.1. Diffusive Mass Transfer

For diffusive mass transfer, $j_B(\mathbf{x}, t|\alpha)$ is given by the integrated diffusive flux over the boundary $\partial\Omega(\alpha)$ of the immobile domain normalized by the immobile volume $V_{im}(\alpha)$, that is

$$j_B(\mathbf{x}, t|\alpha) = -\phi_{im}(\alpha) \frac{D_{im}(\alpha)}{V_{im}(\alpha)} \int_{S_{im}(\alpha)} d\mathbf{f} \cdot \nabla_r g_{im}(\mathbf{r}, t|\alpha). \quad (9)$$

where $S_{im}(\alpha)$ is the boundary surface of and $D_{im}(\alpha)$ and $g_{im}(\mathbf{r}, t|\alpha)$ the diffusion coefficient and concentration distribution in the immobile region of

type α . The latter satisfies the reaction-diffusion equation

$$\frac{\partial g_{im}(\mathbf{r}, t|\alpha)}{\partial t} - D_{im}(\alpha) \nabla_r^2 g_{im}(\mathbf{r}, t|\alpha) = -k_{im}(\alpha) [g_{im}(\mathbf{r}, t|\alpha) - c^{eq}] \quad (10)$$

with the initial boundary conditions

$$g_{im}(\mathbf{r}, t = 0|\alpha) = c^{eq}, \quad g_{im}(\mathbf{r}, t = 0|\alpha)|_{\mathbf{r} \in \partial\Omega(\alpha)} = c_m(\mathbf{x}, t). \quad (11)$$

The average immobile concentration $c_{im}(\mathbf{x}, t|\alpha)$ here is given by

$$c_{im}(\mathbf{x}, t|\alpha) = \frac{1}{V_{im}(\alpha)} \int_{V_{im}(\alpha)} d\mathbf{r} g_{im}(\mathbf{r}, t|\alpha). \quad (12)$$

2.2. First-Order Mass Transfer

For first-order mass transfer between the mobile and immobile regions, the exchange flux between the mobile zones and the immobile zone of type α is given by

$$j_B(\mathbf{x}, t|\alpha) = \frac{\phi_{im}(\alpha)}{\tau(\alpha)} [c_m(\mathbf{x}, t) - c_{im}(\mathbf{x}, t|\alpha)] \quad (13)$$

where $\tau(\alpha)$ is the residence time in the immobile zone. [This mobile-immobile model coupled with first-order degradation reactions, i.e., \$c^{eq} = 0\$ in Eq. \(8\), was studied in Roth and Jury \(1993\) and Das et al. \(2002\)](#)

2.3. Closed Form Equation for the Mobile Concentration

For first-order as well as diffusive mass transfer, the immobile concentration $c_{im}(\mathbf{x}, t|\alpha)$ can be written as a linear functional of the mobile concentration similar to Equation (1d), but which now reads (see Appendix B)

$$c_{im}(\mathbf{x}, t|\alpha) = \int_0^t dt' \varphi_r(t - t'|\alpha) [c_m(\mathbf{x}, t') - c^{eq}] + c^{eq}. \quad (14)$$

The 'reactive' memory function $\varphi_r(t|\alpha)$ is defined by

$$\varphi_r(t|\alpha) = \varphi(t|\alpha) \exp[-k_{im}(\alpha)t], \quad (15)$$

where $\varphi(t|\alpha)$ is the memory function for a non-reactive tracer. The latter depends on the specific (linear) mass transfer mechanism under consideration. For the first-order mass transfer considered above, it is given by

$$\varphi(t|\alpha) = \frac{\exp[-t/\tau(\alpha)]}{\tau(\alpha)}. \quad (16)$$

For diffusive mass transfer into spherical inclusions, it is given by

$$\varphi(t|\alpha) = \mathcal{L}^{-1} \left\{ \frac{3}{\sqrt{s\tau(\alpha)}} \left[\coth \left[\sqrt{s\tau(\alpha)} \right] - \frac{1}{\sqrt{s\tau(\alpha)}} \right] \right\}, \quad (17)$$

where \mathcal{L} stands for Laplace transform, s is the Laplace variable, and $\tau(\alpha) = R(\alpha)^2/D_{im}(\alpha)$ with $R(\alpha)$ the radius of the spherical immobile region $\Omega(\alpha)$. Memory functions for diffusion into immobile regions of other geometries can be found in Haggerty and Gorelick (1995) and Carrera et al. (1998). It has been shown by Haggerty and Gorelick (1995) and Carrera et al. (1998) that the memory function for diffusive mass transfer can be expressed in terms of a suitably chosen superposition of memory functions for first-order mass transfer functions (16).

Inserting (14) into (8) and rearranging terms, we obtain the closed reac-

tive transport equation for the concentration in the mobile zone

$$\begin{aligned} \phi_m \frac{\partial c_m(\mathbf{x}, t)}{\partial t} + \frac{\partial}{\partial t} \int_0^t dt' \varphi_r(t-t') c_m(\mathbf{x}, t') \\ + \nabla \cdot [\mathbf{q}(\mathbf{x}) c_m(\mathbf{x}, t) - \mathbf{D}_m \nabla c_m(\mathbf{x}, t)] = - \int_0^t dt' \kappa(t-t') [c_m(\mathbf{x}, t') - c^{eq}]. \end{aligned} \quad (18a)$$

where we have included the global memory function and the global reaction rate kernel, given by

$$\varphi_r(t) = \int_0^\infty d\alpha \mathcal{P}(\alpha) \phi_{im}(\alpha) \varphi_r(t|\alpha) \quad (18b)$$

$$\kappa(t) = \phi_m k_m \delta(t) + \int_0^\infty d\alpha \mathcal{P}(\alpha) \phi_{im}(\alpha) k_{im}(\alpha) \varphi_r(t|\alpha), \quad (18c)$$

respectively. The system (18) can be seen as an upscaled reactive transport description for the mobile solute that it provides a single (non-local) reactive transport equation characterized by mass transfer and reaction memory kernels. These kernels integrate the dynamics of the complex (subscale) dynamics consisting of mass transfer and reaction in the mobile and immobile regions.

For linear mass transfer between mobile and immobile regions and linear first-order adsorption kinetics in the mobile and immobile regions, it has been shown that the mass transfer and reaction processes can be represented in terms of a single memory function (e.g., Brusseau et al., 1989; Sardin et al., 1991). Here, these processes cannot be represented by a single memory

function, but are manifested in two memory terms, the global memory function (18b) and the reaction kernel (18c)

The effects of chemical and physical heterogeneity as reflected in the distributions of mass transfer rates and kinetic rate constants, respectively, are intimately related in their impact on the effective memory function and reaction rate kernel as manifest in (18b) and (18c). This observation shows that physical and chemical heterogeneity cannot be upscaled separately, that is, mass transfer as expressed by (18b) is impacted on by chemistry and the reaction as expressed by (18c) by mass transfer. Explicit Laplace space solutions of (18a) for different initial and boundary conditions can be found in Appendix C.

3. Breakthrough Curves

In this section we study the solute breakthrough at a control plane perpendicular to the direction of the mean fluid flow. We focus on the solutions for the two end members of the reactive transport problem discussed in the previous section. The first scenario considers a medium that is characterized by a distribution of residence times and a single kinetic rate constant. The second scenario considers a medium characterized by a distribution of reaction rate constants and only a single (first-order) residence time. Mass transfer is assumed to be first-order single rate. Figure 2 illustrates these two limiting cases of possible scenarios. In general, both the mass transfer times and kinetic rate constant should be distributed. We focus on situations for which there is no reaction in the mobile zone, that is $k_m = 0$. For

clarity, we briefly summarize the characteristic times appearing in the following analysis. The diffusive residence time in spherical immobile regions is defined by $\tau_d = R^2/D_{im}$ with R^2 the radius of the immobile zone and D_{im} the immobile diffusion coefficient. The characteristic reaction time scale for is defined by $\tau_r = 1/k_{im}$. The first-order mass transfer time is denoted by τ . The characteristic time scale of the power-law residence time distribution (24) is denoted by τ_0 . The advective peak breakthrough time is defined by $\tau_a = \phi_m x_1/q$. The results for the breakthrough curves in the following subsections are obtained by numerical inverse Laplace transform of the explicit Laplace space solutions given in Appendix D. Furthermore, times are non-dimensionalized by the advective peak time τ_a , length are normalized by the position of the control plane $x_1 = L$. The Peclet number is defined by $Pe = qL/D_m$.

3.1. Multirate Mass Transfer and Uniform Reaction Rate Constant

Here we consider a situation where the sizes and diffusion coefficients of the immobile regions and thus residence times can vary while the porosity and reaction rate constants are the same for all immobile regions. Spatial heterogeneity is represented by a distribution of residence times. Thus, we identify the continuous variable α with the time scale $\tau(\alpha)$, $\alpha = \tau$, so that $\mathcal{P}(\alpha)$ is equated to the distribution of residence times, $\mathcal{P}_\tau(\tau)$. The memory

kernels, (18b) and (18c), simplify to

$$\varphi_r(t) = \phi_{im} \exp[-k_{im}t] \int_0^\infty d\tau \mathcal{P}_\tau(\tau) \varphi(t|\tau), \quad (19)$$

$$\kappa(t) = \phi_m k_m \delta(t) + k_{im} \varphi_r(t), \quad (20)$$

In order to extract the behavior of $\varphi_r(t)$ depending on the specific form of $\mathcal{P}_\tau(\tau)$, we observe that the memory functions for diffusive as well as first-order mass transfer can be written as

$$\varphi(t|\tau) = \frac{\phi[t/\tau]}{\tau}, \quad (21)$$

see, e.g., (15) and (16). Thus, (19) can be rewritten as follows

$$\varphi_r(t) = \phi_{im} \exp[-k_{im}t] \int_0^\infty dx x^{-1} \mathcal{P}_\tau(t/x) \phi(x) \quad (22)$$

with $x = t/\tau$. We note that $\phi(x)$ decreases exponentially fast for $x \gg 1$ and $\mathcal{P}_\tau(t/x)$ goes to zero faster than x (because $\mathcal{P}_\tau(\tau)$ is normalized).

3.1.1. Diffusive Mass Transfer into Uniform Spherical Immobile Regions

First we consider diffusive mass transfer between the mobile region and a single type of spherical immobile regions with a memory function given by (16) and residence time τ_d so that

$$\mathcal{P}_\tau(\tau) = \delta(\tau - \tau_d). \quad (23)$$

where $\tau_d = R^2/D_{im}$ is the diffusion time scale, which measure the time for complete mixing in the immobile zone of radius R . Therefore, a Damköhler

number to compare the reaction time with the time for complete mixing in the immobile zone is $Da_d = k_{im}\tau_d$. Lichtner and Kang (2007) studied the steady state limit of this model. Note that diffusive mass transfer characterized by a single diffusion time scale can be represented by a first-order multirate mass transfer model characterized by a distribution of first-order residence times (e.g., Haggerty and Gorelick, 1995).

Figure 3 shows breakthrough curves of the reactive solute at a control plane at $x_1 = 1$ for different reaction times τ_r . It is clear that the reaction time acts as a cut-off time scale. In fact, the problem contains two cut-off times, namely the residence time scale τ_d and the reaction scale τ_r . The BTC peaks at the advective travel time $\tau_a = \phi_m x_1 / q$. Thereafter, we observe the characteristic 3/2 slope, which is typical for transport under diffusive mass transfer between mobile and immobile regions (e.g., matrix diffusion in fractured media). This behavior is cut off at the minimum of τ_r and τ_d . In short, if immobile regions are uniform, the role of precipitation kinetics is to add a cut-off time.

3.1.2. Distribution of Residence Times

Second, we consider a power-law distribution of residence times

$$\mathcal{P}_\tau(\tau) = \frac{\tau_0^{\beta-1}}{\Gamma(\beta-1)} \frac{\exp(-\tau_0/\tau)}{\tau^\beta}, \quad (24)$$

where $\beta > 1$. This distribution leads to the power law behavior often observed for the tail of BTC, but does not contain a cut-off. We use (30) to represent cases in which the distribution of immobile regions is very broad. In this case, we cannot define a Damköhler number as for the single immobile

zone, which compares the time for complete mixing with the reaction time. At any time, there will be immobile regions which are not completely mixed. Thus, strictly speaking, a Damköhler number cannot be defined. Nevertheless, in the following we define the Damköhler number as $Da_1 = k_{im}\tau_0$, which compares the reaction scale to the characteristic scale τ_0 in (24), which peaks for τ_0/β . For times $\tau \gg \tau_0$ the distribution $\mathcal{P}_\tau(\tau)$ decreases as $\tau^{-\beta}$.

Let us consider the memory function $\varphi_r(t)$ for the power-law (24). Inserting (24) into (22) gives

$$\varphi_r(t) = \phi_{im} \exp[-k_{im}t] \left(\frac{t}{\tau_0}\right)^\beta \frac{1}{\tau_0\Gamma(\beta-1)} \int_0^\infty dx x^{\beta-1} \exp(-\tau_0 x/t) \phi(x). \quad (25)$$

In the limit of $t \gg \tau_0$, $\varphi_r(t)$ can be approximated by

$$\varphi_r(t) = \phi_{im} \exp[-k_{im}t] \left(\frac{t}{\tau_0}\right)^\beta A_\phi, \quad (26)$$

where the constant A_ϕ is given by

$$A_\phi = \frac{1}{\tau_0\Gamma(\beta-1)} \int_0^\infty dx x^{\beta-1} \phi(x). \quad (27)$$

Note that for times larger than τ_0 , the behavior of $\varphi_r(t)$ depends on the specific mass transfer mechanism (diffusive or first-order), only in terms of the constant A_ϕ . For the power-law model, we will be interested in the transport behavior for times that are larger than τ_0 . The behavior will be the same irrespective of the particular mass transfer mechanism. Thus, for the power-law model, we choose for simplicity $\phi(x) = \exp(-x)$ corresponding

to first-order mass transfer. The memory function then reads as

$$\varphi_r(t) = \frac{\phi_{im}\Gamma(\beta)}{\tau_0\Gamma(\beta-1)} \frac{\exp[-k_{im}t]}{(1+t/\tau_0)^\beta}. \quad (28)$$

Note that the exponential term in (28) truncates $\varphi_r(t)$ by the reaction time $\tau_r = k_{im}^{-1}$. Figure 4 shows the flux-averaged concentration at a control plane at $x = 10$ for the above power-law distribution of first-order residence times with $\beta = 3/2$ and different reaction time scales τ_r . For $\tau_r = 10^4$ (a) and 10^5 (b) we can clearly observe the characteristic power-law tail of the breakthrough curves $c_f(x_1, t) \propto t^{-1-\beta}$. Note that the peak is significantly delayed with respect to the advection scale $x_1\phi_m/q = 0.1$ in Figure 4, which reflects that the early arrival solute has mixed within the fast exchange immobile regions. This is consistent with the field observations of Guimera and Carrera (2000) and supports the realism of (24). For decreasing τ_r , the BTCs display a cut-off at the reaction time scale. All breakthrough curves show a peak at τ_a .

3.2. Distribution of Kinetic Rate Parameters and Single Rate First-Order Mass Transfer

We now consider cases in which the reaction rate constants are variable while the immobile diffusion coefficients, immobile domain sizes and the immobile porosities are constant. This means that the residence time is constant $\tau(\alpha) = \tau$ so that the memory function $\varphi(t|\tau)$ is the same for all immobile regions. Therefore, we identify the label α with the immobile reaction rates, $\alpha \equiv k_{im}(\alpha)$, as the immobile regions are uniquely characterized by their

reaction rate constants. The distribution of the immobile regions then is described by the distribution of k_{im} , $\mathcal{P}_k(k_{im})$. In this case the kernels (18b) and (18c) simplify to

$$\varphi_r(t) = \varphi(t|\tau)\phi_{im} \int_0^\infty dk_{im} \mathcal{P}_k(k_{im}) \exp[-k_{im}(\alpha)t] \quad (29)$$

$$\kappa(t) = k_m \delta(t) + \varphi(t|\tau)\phi_{im} \int_0^\infty dk_{im} \mathcal{P}_k(k_{im}) k_{im} \exp[-k_{im}t], \quad (30)$$

For simplicity, we consider single rate first-order mass transfer between mobile and immobile regions as characterized by the memory function (16). Furthermore, we consider a power-law distribution of reaction rate constants similar to (24)

$$\mathcal{P}_k(k_{im}) = \frac{k_{im}^{\beta-1}}{k_0^\beta \Gamma(\beta)} \exp(-k_{im}/k_0). \quad (31)$$

where $1/k_0$ denotes the characteristic reaction time. Inserting the latter into (29) and (30), we obtain for the memory function and reaction kernel

$$\varphi_r(t) = \frac{\varphi(t|\tau)\phi_{im}}{(1+k_0t)^\beta} \quad (32)$$

$$\kappa(t) = k_m \delta(t) + \frac{\Gamma(1+\beta)}{\Gamma(\beta)} \frac{\varphi(t|\tau)\phi_{im}k_0}{(1+k_0t)^{1+\beta}}, \quad (33)$$

Figure 5 illustrates breakthrough curves at the control plane at $x_1 = 1$ for different exponents in the power-law distribution (31) of reaction rates. All breakthrough curves show a maximum at τ_a because this time is much smaller than the characteristic transfer times, which are $\tau = 10^3$ in (a) and 10^4 in (b). For late times, the breakthrough curves are cut-off at τ and decay exponentially fast to zero. At intermediate times $\phi_m \ll t \ll \tau$ the

breakthrough behavior depends on the exponents in the power-law distribution (31) of the reaction rate constants. Note that the tail also displays a power law behavior with the same exponent as that of the reaction rate constants. The smaller the exponent, the larger is the weight of the distribution on small k_{im} -values and the less solute precipitate, that is, the larger is the value of the flux concentration and the flatter is the breakthrough curve.

The mass transfer time scale τ acts as a cut-off scale also in the case of distributed reaction rates, as illustrated in Figure 6, which shows the breakthrough curve for $\beta = 1/2$ for different mass transfer scales τ . The faster the mass exchange between mobile and immobile regions, the less reaction takes place at early times. All curves have a maximum on the advection scale τ_a and decrease then exponentially fast to a point, where the power law behavior starts up. For increasing residence time, the concentration value at this point is decreasing, indicating that less reaction takes place initially if mass exchange is fast. For slow mass transfer, there is more reaction initially. At late times, the concentration decreases slowly according to a power-law that is given by the exponent in (31).

4. Effective Coefficients

An effective (time-dependent) retardation coefficient and an effective reaction rate coefficient can be defined by the time integrals of (18b) and (18c),

respectively

$$R^e(t) = \phi_m + \int_0^\infty d\alpha \mathcal{P}(\alpha) \phi_{im}(\alpha) \int_0^t dt' \varphi(t'|\alpha) \exp[-k_{im}(\alpha)t'] \quad (34)$$

$$k^e(t) = \phi_m k_m + \int_0^\infty d\alpha \mathcal{P}(\alpha) \phi_{im}(\alpha) k_{im}(\alpha) \int_0^t dt' \varphi(t'|\alpha) \exp[-k_{im}(\alpha)t']. \quad (35)$$

Figure 7 illustrates the behavior of the effective rate coefficients (35) for uniform kinetic rate coefficient k_{im} , uniform immobile porosity ϕ_{im} and $k_m = 0$ with (i) first-order MRMT characterized by the residence time distribution (24) for $\beta = 3/2$, and (ii) diffusive mass transfer into spherical immobile zones, see Appendix E. For the power-law first-order mass transfer model (24), we defined the Damköhler number $Da_1 = k_{im}\tau_0$ (see section 3.1), where τ_0 is the characteristic time scale of the power-law distribution. For mass transfer between the mobile and spherical immobile regions, we defined the Damköhler number by $Da_d = k_{im}\tau_d$, where $\tau_d = R^2/D$ is the diffusion time scale in the immobile zone.

The effective rate parameters evolve from 0 at time $t = 0$ to asymptotic values which depend on the value of the respective Damköhler number and are smaller than the volume averaged reaction rate constant

$$k_v = \phi_m k_m + \int_0^\infty d\alpha \mathcal{P}(\alpha) \phi_{im}(\alpha) k_{im}(\alpha) \quad (36)$$

which would be the value measured without mass transfer restrictions, that is, in the limit of very small Damköhler numbers. The time evolution of $k^e(t)$ is determined by the interplay between the characteristic mass transfer

scales and the reaction scales. In Figure 7, time is measured in units of the characteristic transport scales. The $k^e(t)$ evolves on a non-dimensional scale given by the inverse Damköhler number. The dependence of $k^e(t)$ on travel time reflects a scale behavior of the reaction process. The value of the effective rate parameter depends on the measurement scale, that is, on the size of the structures that have been sampled by the solute, which increases with increasing time.

In the long time limit, transport can be described by the advection-diffusion-reaction equation characterized by the effective retardation and reaction rates

$$R^a \frac{\partial c_m(\mathbf{x}, t)}{\partial t} + \nabla \cdot [\mathbf{q}(\mathbf{x}, t)c_m(\mathbf{x}, t) - \mathbf{D}_m \nabla c_m(\mathbf{x}, t)] = -k^a [c_m(\mathbf{x}, t) - c^{eq}], \quad (37)$$

where the asymptotic long-time limits R^a and k^a are given by

$$R^a = \phi_m + \int_0^\infty d\alpha \mathcal{P}(\alpha) \phi_{im}(\alpha) \hat{\varphi} [k_{im}(\alpha) | \alpha] \quad (38)$$

$$k^a = \phi_m k_m + \int_0^\infty d\alpha \mathcal{P}(\alpha) \phi_{im}(\alpha) k_{im}(\alpha) \hat{\varphi} [k_{im}(\alpha) | \alpha]. \quad (39)$$

Specifically for a uniform kinetic rate coefficient in the immobile regions and the power-law model (24) of mass transfer times, the asymptotic rate is given by

$$k^a = \phi_m k_m + \phi_{im} k_{im} \exp(Da_1) Da_1^{\beta-1} \frac{\Gamma(\beta)}{\Gamma(\beta-1)} \Gamma(1-\beta, Da_1). \quad (40)$$

For uniform kinetic rate and diffusion into spherical immobile regions, it is given by

$$k^a = \phi_m k_m + \phi_{im} k_{im} \frac{3}{\sqrt{Da_d}} \left[\coth \left(\sqrt{Da_d} \right) - \frac{1}{\sqrt{Da_d}} \right]. \quad (41)$$

Figure 8 shows the behavior of the asymptotic rates (40) and (41) as a function of Da . In both cases k^a decreases with increasing Damköhler. For the diffusion into a single immobile region this reflects the fact that the solute during the reaction time τ_r can only penetrate to a layer of thickness $\sqrt{2\tau_r D_{im}}$, the rest of the immobile zone cannot contribute to the reaction. For the power-law model this is similar. Only structures with a typical residence time smaller or equal to τ_r contribute to the bulk reactivity. The evolution of the effective rate parameter with travel time, Figure 7, and the dependence of the asymptotic value on the Damköhler number, Figure 8, reflect the scale dependence of the processes. These results quantify the disparity between laboratory and effective field reaction rates. Depending on the Damköhler number; the effective rate can be virtually any fraction of the local rate, which is consistent with the fact that laboratory measured kinetic rates can be ~~order~~ orders of magnitudes larger than their field measured counterparts (e.g., White and Brantley, 2003; Li et al., 2008).

The effective reaction rate $r^e(\mathbf{x}, t)$ is expressed in terms of the right side of (18a) as

$$r^e(\mathbf{x}, t) = \int_0^t dt' \kappa(t - t') [c_m(\mathbf{x}, t') - c^{eq}]. \quad (42)$$

The total precipitated mass at a position \mathbf{x} is given by

$$M(\mathbf{x}, t) = \int_0^t r^e(\mathbf{x}, t), \quad (43)$$

which in the limit of time to infinity is

$$M(\mathbf{x}) = \lim_{t \rightarrow \infty} M(\mathbf{x}, t) = k^a [\hat{c}_m(\mathbf{x}, \lambda) - c^{eq}]_{\lambda=0}. \quad (44)$$

The behavior of the total precipitated mass is identical to the one found in a reactive transport system that is characterized by the effective rate constant k^a .

5. Conclusions

We presented analytical solutions to the problem of transport in a multi-continua medium combined with kinetically controlled reaction using an effective non-local in time transport formalism. The objective was to study the combined effect of physical and chemical heterogeneity (as expressed by distributions of residence times and reaction coefficients in the immobile continua) on the effective reactive transport behavior. The latter was quantified in terms of breakthrough curves of the reacting species as well as in terms of upscaled reaction and transport coefficients (i.e., effective Darcy scale coefficients) that characterize transport and reactions in rocks where mobile and immobile regions can be defined. In short, it turns out that heterogeneity in the transport and reaction parameters cannot be upscaled separately. Upscaled reaction characteristics depend on the physical heterogeneity and

upscaled transport characteristics are impacted on by the chemical heterogeneity.

For first-order or diffusive mass transfers the 'physical' memory function, which quantifies the trapping time distribution in the immobile zone of a non-reactive tracer is replaced by the 'reactive' memory function, $\varphi_r(t)$ accounting for the reactions in the immobile zones,

$$\varphi_r(t) = \int_0^\infty d\alpha \mathcal{P}(\alpha) \phi_{im}(\alpha) \varphi(t|\alpha) \exp[-k_{im}(\alpha)t], \quad (45)$$

where $\mathcal{P}(\alpha)$ is the distribution of immobile zones characterized by the porosity $\phi_{im}(\alpha)$, the effective kinetic coefficient $k_{im}(\alpha)$ and the 'physical' local memory function $\varphi(t|\alpha)$. This expression emphasizes that the effective memory function for reactive transport integrates the effects of the physical and of the chemical heterogeneity: their upscaling cannot be performed separately. The effective coefficients that characterize retardation, $R^e(t)$, and reaction rate, $k^e(t)$, are obtained as

$$R^e(t) = \phi_m + \int_0^\infty d\alpha \mathcal{P}(\alpha) \phi_{im}(\alpha) \int_0^t dt' \varphi(t'|\alpha) \exp[-k_{im}(\alpha)t'] \quad (46)$$

$$k^e(t) = \phi_m k_m + \int_0^\infty d\alpha \mathcal{P}(\alpha) \phi_{im}(\alpha) k_{im}(\alpha) \int_0^t dt' \varphi(t'|\alpha) \exp[-k_{im}(\alpha)t']. \quad (47)$$

Equation ~~(46)~~ (46) shows that, while diffusion into immobile zones causes retardation in solute transport (with an asymptotic value scaling as $\phi_{im} + \phi_m$), the effective retardation can be greatly reduced in the case of reactive solute. It follows that the breakthrough curves (i.e. the time-resolved concentration

measured at a given distance from the inlet) depend on both the distribution of the residence times due to diffusion and the distribution of the kinetic rate coefficients. As a result it is not straightforward to infer parameters for a reactive tracer test from a non-reactive one because the mass transfer memory function for the reactive problem cannot be obtained independent from the reaction and the reactive part cannot be obtained independent from mass transfer.

The dependence of $k^e(t)$ on travel time reflects a scale behavior of the reaction process. The value of the effective rate parameter depends on the measurement scale, that is on the size of the structures that have been sampled by the solute. The size of the structures sampled by the solute increases with increasing time. The concentration of the chemical reactions in immobile regions, which may occur in many natural rocks displaying complex pore structures, explains the often observed discrepancy between the effective kinetics deduced from field scale data (as approximated by our multicontinuum approach) and those measured at laboratory scale using grinded material. As the rock is grinded it is expected that mass transfer limitations due long lasting incomplete mixing in the immobile domain are reduced. This situation corresponds to the decrease of the diffusion time scale τ_d triggered by the decrease of the immobile zone radius R ($\tau_d \propto R^2$). The reaction rate constant deduced from laboratory experiments k_{lab} tends to equal the volumetric average k_v of the distributed k_{im} values ($k_m = 0$):

$$k_{lab} \approx k_v = \int_0^{\infty} d\alpha \mathcal{P}(\alpha) \phi_{im}(\alpha) k_{im}(\alpha) < k_e, \quad (48)$$

where $k_v \ll k_e$ (compare (48) with (39)). Hence, as ~~grinding rocks acts as decreasing grinding the rocks decreases~~ the effective Damköhler number, this scaling must be taken into account when using kinetic coefficient values measured using laboratory reactors for parameterizing mass transfers models at reservoir scale.

Acknowledgments

The authors thank the editor Al Valocchi ~~and two anonymous reviewers,~~ Insa Neuweiler and an anonymous reviewer for their insightful comments and suggestions. The authors acknowledge the support of ~~CIUDEN~~, the ANR project COLINER and the European Union project MUSTANG and CIUDEN.

Appendix A. Linearization of the Reaction Rate

The objective of this Appendix is to discuss cases in which the rate of a kinetic reaction can be approximated as a linear (affine, strictly speaking) function. Linear approximations are quite frequently adopted for pollutants degradation when the rate limiting factor is the pollutant concentration. Here we analyze mineral dissolution precipitation reactions (4), where the rate (3) can be approximated as:

$$r = -\vartheta\sigma \left(1 - \frac{c_A c_B}{K}\right) = \frac{\vartheta\sigma c_B}{K} \left(c_A - \frac{K}{c_B}\right), \quad (\text{A.1})$$

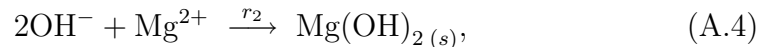
where K is the equilibrium constant for reaction (4) and c_A and c_B are the concentrations of reacting species. This expression can be linearized in

several cases. The most immediate one is the case where c_B is very large, so that its value will not be significantly affected by mineral dissolution or precipitation. Assuming c_B constant in (A.1) leads to:

$$r = k (c_A - c_A^{eq}), \quad (\text{A.2})$$

where $k = \vartheta \sigma c_B / K$ and $c_A^{eq} = K / c_B$. In general, c_B cannot be assumed constant. In fact, both c_A and c_B may be affected by other reactions. In such cases, the problem becomes multicomponent and linearization consists of the following steps: (i) Decouple conservative and non-conservative components using the approach of Molins et al. (2004); (ii) Solve for conservative components; (iii) Write the transport equation for non-conservative components using the approach of Donado et al. (2009); (iv) Linearize the reaction rates by means of a Taylor series expansion; (v) Test the validity of linearization.

The method is applied here for the case of brucite $[\text{Mg}(\text{OH})_2]$ precipitation, which can be simplified as consisting of two reactions:



where r_1 and r_2 represent the rates ($\text{mol}/\text{s}/\text{m}_{rock}^3$) at which the products (H_2O and $\text{Mg}(\text{OH})_2$, respectively) evolve into reactants. The reactive transport problem can be written as:

$$L(c_{\text{H}}) = -r_1 \quad (\text{A.5})$$

$$L(c_{\text{OH}}) = -r_1 - 2r_2 \quad (\text{A.6})$$

$$L(c_{\text{Mg}}) = -r_2, \quad (\text{A.7})$$

where $L(\cdot)$ represents the transport operator. The first step (e.g., Molins et al., 2004) consists of eliminating r_1 and r_2 , which, in this case, simply consists of subtracting (A.5) and (A.7), multiplied by 2, from (A.6), which yields:

$$L(n) = 0, \quad (\text{A.8})$$

where $n = c_{2\text{Mg}} - c_{\text{OH}} + c_{\text{H}}$, which can be solved by any transport solver. Given n and using the mass action law for water, one can solve for c_{OH} as:

$$c_{\text{OH}} = \left[(2c_{\text{Mg}} - n) + \sqrt{(n - c_{\text{Mg}})^2 + 4K_w} \right] / 2, \quad (\text{A.9})$$

where $K_w = c_{\text{H}}^{eq} c_{\text{OH}}^{eq} = 10^{-14}$ is the equilibrium constant for reaction (A.3).

Let us now look at the reaction rate

$$r = -\vartheta\sigma \left(1 - \frac{c_{\text{OH}}^2 c_{\text{Mg}}}{K_{br}} \right). \quad (\text{A.10})$$

A Taylor expansion in c_{Mg} about a certain concentration $c_{\text{Mg}}^{(0)}$ gives

$$r \approx r^{(0)} + \frac{\partial r^{(0)}}{\partial c_{\text{Mg}}} \left(c_{\text{Mg}} - c_{\text{Mg}}^{(0)} \right), \quad (\text{A.11})$$

where K_{br} is brucite equilibrium constant and $r^{(0)}$ represents the reaction rate for $c_{\text{Mg}}^{(0)}$. Using (A.9) for c_{OH} , derivatives of (A.10) with respect to c_{Mg} to obtain $\frac{\partial r^{(0)}}{\partial c_{\text{Mg}}}$, and substituting the resulting expression in the Taylor expansion (A.10), yields:

$$r \approx C' c_n^{(0)} - C c_n^{(0)} \vartheta\sigma \left[c_{\text{Mg}} - c_{\text{Mg}}^{(0)} \right], \quad (\text{A.12})$$

where C and C' are constants and $c_n^{(0)} = c_{2\text{Mg}}^{(0)} - c_{\text{OH}}^{(0)} + c_{\text{H}}^{(0)}$. Performing the Taylor expansion for $c_{\text{Mg}}^{(0)} \equiv c_{\text{Mg}}^{eq}$ gives:

$$r \approx -C(c_n^{eq}) \vartheta\sigma \left(c_{\text{Mg}} - c_{\text{Mg}}^{eq} \right) \quad (\text{A.13})$$

with $c_n^{eq} = c_{2Mg}^{eq} - c_{OH}^{eq} + c_H^{eq}$, where the equilibrium concentrations (c_i^{eq}) are given by the mass action laws, given the equilibrium constants K_{br} and K_w .

Appendix B. Diffusive Mass Transfer: Concentration in the Immobile Regions

In order to solve (10) for the immobile concentration, we express $g_{im}(\mathbf{r}, t|\alpha)$ as

$$g_{im}(\mathbf{r}, t|\alpha) = h(\mathbf{r}, t|\alpha) \exp[-k(\alpha)_{im}t] + c^{eq}, \quad (\text{B.1})$$

where $h(\mathbf{r}, t|\alpha)$ satisfies

$$\frac{\partial h(\mathbf{r}, t|\alpha)}{\partial t} - D_{im}(\alpha)\nabla^2 h(\mathbf{r}, t|\alpha) = 0 \quad (\text{B.2})$$

with the initial boundary conditions

$$h(\mathbf{r}, t = 0|\alpha) = 0, \quad h(\mathbf{r}, t|\alpha)|_{\mathbf{r} \in \partial\Omega(\alpha)} = [c_m(x, t) - c^{eq}] \exp[k_{im}(\alpha)t]. \quad (\text{B.3})$$

$h(\mathbf{r}, t|\alpha)$ can be expressed by the Green function $f(\mathbf{r}, t|\alpha)$ of the diffusion equation (B.2) for the initial condition $f(\mathbf{r}, t = 0|\alpha) = 0$ and the boundary condition $f(\mathbf{r}, t|\alpha)|_{\mathbf{r} \in \partial\Omega(\alpha)} = \delta(t)$ as

$$h(\mathbf{r}, t|\alpha) = \int_0^t dt' f(\mathbf{r}, t - t'|\alpha) [c_m(x, t') - c^{eq}] \exp[k_{im}(\alpha)t']. \quad (\text{B.4})$$

Using (B.1) and (B.4), we can write $g_{im}(\mathbf{r}, t|\alpha)$ as

$$g_{im}(\mathbf{r}, t|\alpha) = \int_0^t dt' f(\mathbf{r}, t - t') [c_m(x, t') - c^{eq}] \exp[-k_{im}(\alpha)(t - t')] + c^{eq}, \quad (\text{B.5})$$

Inserting (B.5) into (12) gives (14). The memory function $\varphi(t|\alpha)$ is defined in terms of the Green function $f(\mathbf{r}, t|\alpha)$

$$\varphi(t|\alpha) = \frac{1}{V_{im}(\alpha)} \int_{V_{im}(\alpha)} d\mathbf{r} f(\mathbf{r}, t|\alpha), \quad (\text{B.6})$$

which is identical to the definition for a non-reactive tracer.

Appendix C. Mobile Concentration

In the following, we derive some solutions for the one-dimensional non-local advection-diffusion-reaction equation (18a). To this end, we define the auxiliary function h_m by

$$c_m = \exp\left(-\frac{k_m t}{\phi_m}\right) h_m + c^{eq}. \quad (\text{C.1})$$

We obtain by inserting (C.1) into (18a)

$$\begin{aligned} \phi_m \frac{\partial h_m}{\partial t} + q \frac{\partial h_m}{\partial x_1} - D_m \frac{\partial^2 h_m}{\partial x_1^2} = \\ - \int_0^\infty d\alpha \mathcal{P}(\alpha) \phi_{im}(\alpha) \left[\frac{\partial}{\partial t} + k_{im}(\alpha) \right] \int_0^t dt' m(t-t'|\alpha) h_m(x_1, t'), \end{aligned} \quad (\text{C.2})$$

where we defined the memory function

$$m(t|\alpha) = \varphi(t|\alpha) \exp[-\Delta k(\alpha)t] \quad (\text{C.3})$$

and $\Delta k(\alpha) = k_{im}(\alpha) - k_m/\phi_m$. The Laplace transform of the latter is given by

$$\hat{m}(\lambda|\alpha) = \hat{\varphi}(\lambda + \Delta k_i|\alpha). \quad (\text{C.4})$$

Appendix C.1. Pulse-Injection Into the Mobile Region

We specify vanishing mobile concentration at the domain boundaries at infinity and the initial condition $c_m(x_1, t = 0) = \rho(x_1) + c^{eq}$. The initial condition for h_m is given by $h_m(x_1, t = 0) = \rho(x_1)$.

The latter equation reads in Laplace space as

$$\begin{aligned} \phi_m \lambda \hat{h}_m + q \frac{\partial \hat{h}_m}{\partial x_1} - D_m \frac{\partial^2 \hat{h}_m}{\partial x_1^2} &= \rho(x_1) \\ - \int_0^\infty d\alpha \mathcal{P}(\alpha) \phi_{im}(\alpha) [\lambda + k_{im}(\alpha)] \hat{m}(\lambda|\alpha) \hat{h}_m(x_1, \lambda), \end{aligned} \quad (\text{C.5})$$

For a delta initial injection we obtain

$$\hat{h}_m^\delta(x_1, \lambda) = \frac{\exp \left[-\frac{q}{2D} \left\{ \sqrt{x_1^2 + 4x_1^2 \frac{\hat{M}(\lambda) D_m}{q^2}} - x_1 \right\} \right]}{q \sqrt{1 + 4 \frac{\hat{M}(\lambda) D_m}{q^2}}}, \quad (\text{C.6})$$

where we defined

$$\hat{M}(\lambda) = \phi_m \lambda + \int_0^\infty d\alpha \phi_{im}(\alpha) [\lambda + k_{im}(\alpha)] \hat{m}(\lambda|\alpha) \quad (\text{C.7})$$

For a square-pulse, i.e.,

$$\rho(x_1) = C_0 \theta(a - |x_1'|), \quad (\text{C.8})$$

the solution for \hat{h}_m is given by

$$\hat{h}_m(x_1, \lambda) = C_0 \int_{-\infty}^\infty dx_1' h_m^\delta(x_1 - x_1', \lambda) \theta(a - |x_1'|) = C_0 \int_{-a}^a dx_1' h_m^\delta(x_1 - x_1', \lambda). \quad (\text{C.9})$$

The Laplace space solution of the mobile concentration then reads as

$$\hat{c}_m(x_1, \lambda) = \hat{h}_m(x_1, \lambda + k_m/\phi_m) + c^{eq}/\lambda. \quad (\text{C.10})$$

Appendix C.2. Flux Boundary Conditions

The flux boundary conditions are given by

$$\left[c - D_m \frac{\partial c_m}{\partial x_1} \right]_{x_1=0} = j(t) \quad (\text{C.11})$$

and in Laplace space as

$$\left[q\hat{c}_m - D_m \frac{\partial \hat{c}_m}{\partial x_1} \right]_{x_1=0} = \hat{j}. \quad (\text{C.12})$$

For the auxiliary function $h_m(x_1, t)$ this implies

$$\left[qh_m - D_m \frac{\partial h_m}{\partial x_1} \right]_{x_1=0} = [j(t) - c^{eq}q] \exp(-k_m t / \phi_m) \quad (\text{C.13})$$

and in Laplace space

$$\left[q\hat{h}_m - D_m \frac{\partial \hat{h}_m}{\partial x_1} \right]_{x_1=0} = \hat{j}(\lambda - k_m / \phi_m) - \frac{qc^{eq}}{\lambda - k_m / \phi_m}. \quad (\text{C.14})$$

The solution for h_m in Laplace space is given by

$$h_m = B \exp(Ax_1), \quad A = \frac{q}{2D_m} \left[1 - \sqrt{1 + \frac{4D_m \hat{M}(\lambda)}{q^2}} \right] \quad (\text{C.15})$$

The parameter B we obtain by inserting the latter into (C.14)

$$B = \frac{\hat{j}(\lambda - k_m / \phi_m) - \frac{qc^{eq}}{\lambda - k_m / \phi_m}}{q - \frac{q}{2} \left[1 - \sqrt{1 + \frac{4D_m \hat{M}(\lambda)}{q^2}} \right]} \quad (\text{C.16})$$

As in the previous section, we consider a pulse flux input of duration τ

$$j(t) = c^{eq}q + (c_B - c^{eq})q\tau\delta_\tau(t), \quad (\text{C.17})$$

where $\delta_\tau(t)$ is the unit impulse function defined by (D.8).

Thus, we obtain for the mobile concentration the following expression

$$\hat{c}_m(x_1, \lambda) = (c_B - c^{eq}) \frac{2[1 - \exp(-\lambda\tau)]}{\lambda \left\{ 2 - \left[1 - \sqrt{1 + \frac{4D_m \hat{M}(\lambda + k_m/\phi_m)}{q^2}} \right] \right\}} \times \exp \left[\frac{qx_1}{2D_m} \left(1 - \sqrt{1 + \frac{4D_m \hat{M}(\lambda + k_m/\phi_m)}{q^2}} \right) \right] + \frac{c^{eq}}{\lambda}. \quad (\text{C.18})$$

Appendix D. Flux-Averaged Concentration

In the following we will focus on the flux averaged concentration at a control plane Ω_c perpendicular to the mean flow at the position x_1 . It is defined by Kreft and Zuber (1978)

$$c_f(x_1, t) = \left[1 - \frac{D_L}{q} \frac{\partial}{\partial x_1} \right] \int_{\Omega_c} d^{d-1}x c_m(\mathbf{x}, t). \quad (\text{D.1})$$

The flux concentration satisfies the one-dimensional version of (18a) as can be verified by inspection. Explicit Laplace space solutions for $c_f(x_1, t)$ are given in the following for flux-boundary conditions in a semi-infinite transport domain.

We consider the semi-infinite plain $x_1 > 0$. We consider the flux-boundary conditions (C.11). According to (D.1), this implies for the flux averaged concentration $c_f(x_1, t)$

$$c_f(x_1 = 0, t) = C(t), \quad \lim_{x_1 \rightarrow \infty} c_f(x_1, t) = c^{eq} \quad (\text{D.2})$$

and the initial condition $c_f(x_1, t = 0) = c^{eq}$. As outlined above, $c_f(x_1, t)$ satisfies the same equation as the mobile concentration $c_m(x_1, t)$. Thus, in order to solve for $c_f(x_1, t)$ we employ the same method as above and express

$c_f(x_1, t)$ in terms of the auxiliary function $h_m(x_1, t)$, see (C.1). The boundary conditions for the auxiliary function $h_m(x_1, t)$ then are given by

$$h_m(x_1 = 0, t) = [C(t) - c^{eq}] \exp(k_m/\phi_m t), \quad \lim_{x_1 \rightarrow \infty} h_m(x_1, t) = 0 \quad (\text{D.3})$$

and the initial condition is $h_m(x_1, t = 0) = 0$.

We then obtain for the Laplace transform $\hat{h}_m(x_1, \lambda)$

$$\hat{M}(\lambda) \hat{h}_m(x_1, \lambda) + q \frac{\partial \hat{h}_m}{\partial x_1} - D_m \frac{\partial^2 \hat{h}_m}{\partial x_1^2} = 0. \quad (\text{D.4})$$

The boundary conditions are

$$\hat{h}_m(x_1 = 0, \lambda) = \hat{C}(\lambda - k_m/\phi_m) - \frac{c^{eq}}{\lambda - k_m/\phi_m}, \quad \lim_{x_1 \rightarrow \infty} \hat{h}_m(x_1, \lambda) = 0. \quad (\text{D.5})$$

Using the exponential Ansatz $h_m = B \exp(Ax_1)$, we obtain the solution

$$\begin{aligned} \hat{h}_m(x_1, \lambda) &= \left[\hat{C}(\lambda - k_m/\phi_m) - \frac{c^{eq}}{\lambda - k_m/\phi_m} \right] \\ &\times \exp \left[\frac{qx_1}{2D_m} \left(1 - \sqrt{1 + \frac{4D_m \hat{M}(\lambda)}{q^2}} \right) \right]. \end{aligned} \quad (\text{D.6})$$

As boundary conditions, we consider pulse of $c_B = \text{const.}$ in the time interval $[0, \tau]$ and $C(t) = c^{eq}$ for $t \geq \tau$,

$$C(t) = c^{eq} + (c_B - c^{eq}) \tau \delta_\tau(t), \quad (\text{D.7})$$

where $\delta_\tau(t)$ is the unit impulse function defined by

$$\delta_\tau(t) = \begin{cases} 0, & t < 0 \\ \frac{1}{\tau}, & 0 \leq t < \tau \\ 0, & t > \tau \end{cases} \quad (\text{D.8})$$

The Laplace transform of the unit impulse function is given by

$$\hat{\delta}_\tau(\lambda) = \frac{[1 - \exp(-\lambda\tau)]}{\lambda\tau}. \quad (\text{D.9})$$

Thus, we obtain for the Laplace transform of the mobile concentration by combining (C.10), (D.6), and (D.9)

$$\begin{aligned} \hat{c}_f(x_1, \lambda) &= (c_B - c^{eq}) \frac{1 - \exp(-\lambda\tau)}{\lambda} \\ &\times \exp \left[\frac{qx_1}{2D_m} \left(1 - \sqrt{1 + \frac{4D_m \hat{M}(\lambda + k_m/\phi_m)}{q^2}} \right) \right] + \frac{c^{eq}}{\lambda}. \end{aligned} \quad (\text{D.10})$$

Appendix E. Effective Reaction Rate Coefficient

The time behavior for the effective rate coefficients displayed in Figure 7 was obtained as follows. First, the local rate coefficient k_{im} is set constant. For the first-order MRMT model with the power-law residence time distribution (24) and $\beta = 3/2$, the resulting expression can be integrated explicitly and gives

$$\begin{aligned} k^e(t) &= \phi_{im} k_{im} - \phi_{im} k_{im} \frac{\exp(-Da_1 t/\tau_0)}{\sqrt{t/\tau_0 + 1}} \\ &+ \phi_{im} k_{im} \sqrt{\pi Da_1} \exp(Da_1) \left[\text{erf} \left(\sqrt{Da_1} \right) - \text{erf} \left(\sqrt{t/\tau_0 + 1} \sqrt{Da_1} \right) \right]. \end{aligned} \quad (\text{E.1})$$

For diffusive mass transfer into spherical regions, we set $\alpha = \tau_d$ and use for $\varphi(t|\alpha)$ expression (17). Thus, we obtain the following Laplace space expression for the effective rate $k^e(t)$

$$\hat{k}^e(s) = \phi_{im} k_{im} \frac{3}{\sqrt{s\tau_d + Da_1}} \left[\coth \left[\sqrt{s\tau_d + Da_d} \right] - \frac{1}{\sqrt{s\tau_d + Da_d}} \right]. \quad (\text{E.2})$$

The results displayed in Figure 7b are obtained by inverse Laplace transform of this expression.

Aagaard, P., Helgeson, H. C., 1982. Thermodynamic and kinetic constraints on reaction rates among minerals and aqueous solutions: I. theoretical considerations. *American Journal of Science* 282, 237–285.

Battiato, I., Tartakovsky, D. M., Tartakovsky, A. M., Scheibe, T., 2009. On breakdown of macroscopic models of mixing-controlled heterogeneous reactions in porous media. *Adv. Water Resour.* 32, 1664–1673.

Berkowitz, B., Klafter, J., Metzler, R., Scher, H., 2002. Physical pictures of transport in heterogeneous media: Advection-dispersion, random-walk, and fractional derivative formulations. *Water Resour. Res.* 38 (10), 1191.

Brusseau, M. L., Jessup, R. E., Rao, P. S. C., 1989. Modeling the transport of solutes influenced by multiprocess nonequilibrium. *Water Resour. Res.* 25, 1971–1988.

Carrera, J., Sánchez-Vila, X., Benet, I., Medina, A., Galarza, G., Guimerà, J., 1998. On matrix diffusion: formulations, solution methods, and qualitative effects. *Hydrogeology Journal* 6, 178–190.

Cirpka, O. A., Kitanidis, P. K., 2000. An advective-dispersive streamtube approach for the transfer of conservative tracer data to reactive transport. *Water Resour. Res.* 36, 1209–1220.

- Dentz, M., Berkowitz, B., 2003. Transport behavior of a passive solute in continuous time random walks and multirate mass transfer. *Water Resour. Res.* 39 (5), 1111.
- Donado, L. D., Sanchez-Vila, X., Dentz, M., Carrera, J., Bolster, D., 2009. Multi-component reactive transport in multi-continuum media. *Water Resour. Res.* 45, W11402.
- Edwards, D. A., Shapiro, M., Brenner, H., 1993. Dispersion and reaction in two-dimensional model porous media. *Phys. Fluids A* 5, 837–848.
- Espinoza, C., Valocchi, A. J., 1997. Stochastic analysis of one-dimensional transport of kinetically adsorbing solutes in chemically heterogeneous aquifers. *Water Resour. Res.* 33, 2429–2445.
- Ginn, T. R., 2001. Stochastic-convective transport with nonlinear reactions and mixing: finite streamtube ensemble formulation for multicomponent reaction systems with intra-streamtube dispersion. *J. Contam. Hydrol.* 47 (1-2), 1–28.
- Gouze, P., Melean, Z., Le Borgne, T., Dentz, M., Carrera, J., 2008. Non-fickian dispersion in porous media explained by heterogeneous microscale matrix diffusion. *Water Resour. Res.* 44, W11416.
- Guimera, J., Carrera, J., 2000. A comparison of hydraulic and transport parameters measured in low-permeability fractured media. *J. Contam. Hydrol.* 41, 261–281.

- Haggerty, R., Gorelick, S. M., 1995. Multiple-rate mass transfer for modeling diffusion and surface reactions in media with pore-scale heterogeneity. *Water Resour. Res.* 31 (10), 2383–2400.
- Haggerty, R., McKenna, S. A., Meigs, L. C., 2000. On the late time behavior of tracer test breakthrough curves. *Water Resour. Res.* 36 (12), 3467–3479.
- Hornung, U., 1997. *Homogenization and Porous Media*. Springer-Verlag New York, Inc.
- Hu, B. X., Cushman, J. H., Deng, F.-W., 1997. Nonlocal reactive transport with physical, chemical, and biological heterogeneity. *Advances in Water Resources* 20 (5-6), 293 – 308.
- Kechagia, P. E., Tsimpanogiannis, I. N., Yortsos, Y. C., Lichtner, P. C., 2002. On the upscaling of reaction-transport processes in porous media with fast or finite kinetics. *Chemical Engineering Science* 57 (13), 2565 – 2577.
- Kreft, A., Zuber, A., 1978. On the physical meaning of the dispersion equation and its solutions for different initial and boundary conditions. *Chem. Eng. Sci.* 33, 1471–1480.
- Li, L., Peters, C. A., Celia, M. A., 2006. Upscaling geochemical reaction rates using pore-scale network modeling. *Adv. Water Resour.* 29.
- Li, L., Peters, C. A., Celia, M. A., 2007. Effects of mineral spatial distribution on reaction rates in porous media. *Water Resour. Res.* 43, W01419.

- Li, L., Steefel, C. I., Yang, L., 2008. Scale dependence of mineral dissolution rates within single pores and fractures. *Geochim. Cosmochim. Acta* 72, 360–377.
- Lichtner, P. C., Kang, Q., 2007. Upscaling pore-scale reactive transport equations using a multiscale continuum formulation. *Water Resour. Res.* 43, W12S15.
- Lichtner, P. C., Tartakovsky, D. M., 2003. Stochastic analysis of effective rate constant for heterogeneous reactions. *Stoch. Env. Res. Risk Ass.* 17, 419–429.
- Liu, C., Zachara, J. M., Qafoku, N. P., Wang, Z., 2008. Scale-dependent desorption of uranium from contaminated subsurface sediments. *Water Resour. Res.* 44, W08413.
- Maloszewski, P., Zuber, A., 1985. On the theory of tracer experiments-rocks with a porous matrix. *J. Hydrol.* 79, 333–358.
- Meile, C., Tuncay, K., 2006. Scale dependence of reaction rates in porous media. *Advances in Water Resources* 29 (1), 62–71.
- Molins, S., Carrera, J., Ayora, C., Saaltink, M. W., 2004. A formulation for decoupling components in reactive transport problems. *Water Resour. Res.* 40 (10), W10301.
- Neretnieks, I., 1980. Diffusion in the rock matrix: an important factor in radionuclide retardation? *J. Geophys. Res.* 85, 4379–4397.

- Quintard, M., Whitaker, S., 1994. Convection, dispersion and interfacial transport of contaminants: Homogeneous media. *Adv. Water Resour.* 17, 221–239.
- Salamon, P., Fernàndez-Garcia, D., Gómez-Hernández, J. J., 2007. Modeling tracer transport at the made site: The importance of heterogeneity. *Water Resour. Res.* 43, W08404.
- Sardin, M., Schweich, D., Leij, F. J., van Genuchten, M. T., 1991. Modeling the nonequilibrium transport of linearly interacting solutes in porous media: A review. [Water Resour. Res.](#) 27 (9), 2287–2307.
- Schumer, R. D., Benson, M., Meerschaert, M., Baeumer, B., 2003. Fractal mobile/immobile solute transport. *Phys. Rev. E* 39 (10), 1296.
- Seeboonruang, U., Ginn, T. R., 2006. Upscaling heterogeneity in aquifer reactivity via exposure-time concept: Forward model. *J. Cont. Hydrol.* 84, 127–154.
- Silva, O., Carrera, J., Kumar, S., Dentz, M., Alcolea, A., Willmann, M., 2009. A general real-time formulation for multi-rate mass transfer problems. *Hydrol. Earth Syst. Sci. Discuss.* 6, 2415–2449.
- Steeffel, C. I., DePaolo, D. J., Lichtner, P. C., 2005. Reactive transport modeling: An essential tool and a new research approach for the earth sciences. *Earth and Planetary Science Letters* 240, 539–558.

- Tsang, Y., Tsang, C. F., Hale, F. V., Dverstorp, B., 1996. Tracer transport in a stochastic continuum model of fractured media. *Water Resour. Res.* 32, 3077–3092.
- Valocchi, A. J., 1990. Use of temporal moment analysis to study reactive solute transport in aggregated porous media. *Geoderma* 46, 233–247.
- Villiermaux, J., 1987. Chemical engineering approach to dynamic modeling of linear chromatography, a simple method for representing complex phenomena from simple concepts. *J. Chromatogr.* 406, 11–26.
- Whitaker, S., 1999. *The Method of Volume Averaging*. Kluwer Academic Publishers.
- White, A. F., Brantley, S. L., 2003. The effect of time on the weathering of silicate minerals: why do weathering rates differ in the laboratory and in the field? *Chem. Geol.* 3–4, 479–506.
- Willmann, M., Carrera, J., Sanchez-Vila, X., 2008. Transport upscaling in heterogeneous aquifers: What physical parameters control memory functions? *Water Resour. Res.* 44, W12437.
- Willmann, M., Carrera, J., Sanchez-Vila, X., Silva, O., Dentz, M., 2010. Coupling of mass transfer and reactive transport for non-linear reactions in heterogeneous media,. *Water Resour. Res.*, doi:10.1029/2009WR00773.

Figure 1: X-ray microtomography cross section of a pure calcite limestone imaged at different resolutions. Left, porosity map (diameter 1 cm; resolution $5\mu m$). Right, processed image ($600 \times 600 \mu m$, resolution $1\mu m$) showing the mobile domain (in white) and the micro-porosity distribution in the immobile domain formed by clusters of distinctly different size (grey scale). Zones in black are areas unconnected with the immobile domain (porosity lower than the percolation threshold, see also Gouze et al. (2008)).

Figure 2: Conceptual models of matrix diffusion and reaction. The two directions indicated in the figure stand for chemical ($\mathcal{P}(k_{im})$, distribution of kinetic rate coefficient) and physical heterogeneity ($\mathcal{P}(R)$ and $\mathcal{P}(\phi_{im})$, the distributions of inclusion sizes and porosity). The CT scan of the rock illustrates the non-resolved subscale. The different sphere sizes stand for the different types of heterogeneity that are unified in the medium, as indicated by the ellipse in the lower left corner. The two limiting cases discussed in Section 3, consider (1) a medium characterized by a distribution of residence times (e.g. distributed sphere sizes and/or porosity) and a single kinetic rate constant and (2) medium characterized by a distribution of reaction rate constants with a single residence time (e.g. all the spheres have the same radius and porosity).

Figure 3: Breakthrough curves for transport under diffusive mass transfer into immobile regions with uniform chemical properties characterized by the single reaction time scale $\tau_r = 1/k_{im}$. (a) Diffusion in the immobile region is characterized $\tau_d = 10^4$, porosities are $\phi_m = 10^{-1}$, $\phi_{im} = 10^{-2}$, and the reaction times are $\tau_r = 10^5, 10^2, 1$; (b) $\tau_d = 10^5$, porosities are $\phi_m = 10^{-2}$, $\phi_{im} = 10^{-1}$, and the reaction times $\tau_r = 10^6, 10^3, 10$. BTCs are computed at $x_1 = 1$ for $Pe = 10^2$. The curves with (a) $\tau_r = 10^5$ and (b) $\tau_r = 10^6$ are practically indistinguishable from the ones for a conservative solute.

Figure 4: Breakthrough curves for transport in a medium characterized by immobile regions, whose residence time distribution follows (24) with $\beta = 3/2$ and (a) $\tau_0 = 10^{-2}$ and (b) $\tau_0 = 10^{-1}$. The chemical properties in the immobile regions are uniform and characterized by the single reaction time τ_r . Results are presented for (a) $\phi_m = 10^{-1}$ and $\phi_{im} = 10^{-2}$, characteristic reaction times of $\tau_r = 10^4, 10^2, 1$; (b) $\phi_m = 10^{-2}$ and $\phi_{im} = 10^{-1}$ $\tau_r = 10^5, 10^3, 10$. BTCs are computed at $x_1 = 1$ for $Pe = 10^2$. In the displayed time range, the curves with (a) $\tau_r = 10^4$ and (b) $\tau_r = 10^5$ are practically indistinguishable from the ones for a conservative solute.

Figure 5: Breakthrough curves for transport in a medium characterized by immobile regions, whose physical properties are uniform (mass transfer modeled as first-order with residence time (a) $\tau = 10^3$ and (b) $\tau = 10^4$), and whose chemical properties are distributed. The kinetic rate coefficients are distributed according to (31) for $\beta = 1/4$ and $3/4$ with (a) $k_0 = 10^2$ and (b) $k_0 = 10$. Results are presented for (a) $\phi_m = 10^{-1}$ and $\phi_{im} = 10^{-2}$, (b) $\phi_m = 10^{-2}$ and $\phi_{im} = 10^{-1}$. BTCs are computed at $x_1 = 1$ for $Pe = 10^2$. The dashed line denotes the breakthrough curve for a non-reactive solute.

Figure 6: Breakthrough curves for transport in a medium characterized by immobile regions whose chemical properties are distributed. The kinetic rate coefficients are distributed according to (31) for $\beta = 1/2$, (a) $k_0 = 10^2$ and (b) $k_0 = 10$. The physical properties are uniform, which is modeled by a single rate first-order mass transfer. Results are presented for (a) $\phi_m = 10^{-1}$ and $\phi_{im} = 10^{-2}$, and residence times $\tau = 10, 10^2, 10^3$ and (b) $\phi_m = 10^{-2}$ and $\phi_{im} = 10^{-1}$ and residence times $\tau = 10^2, 10^3, 10^4$. BTCs are computed at $x_1 = 1$ for $Pe = 10^2$.

Figure 7: Effective reaction rate coefficients for uniform reaction rate coefficient and (a) the first-order mass transfer model for the power-law distribution (24) for $\beta = 3/2$ and $Da = 10^{-3}, 10^{-2}, 10^{-1}$ and (b) the diffusive mass transfer model for $Da = 1, 10, 10^2$.

Figure 8: Asymptotic effective reaction rate coefficients for uniform kinetic rate coefficient and (solid line) first-order mass transfer with the power-law residence time distribution (24) with $\beta = 3/2$, (40), and (dashed line) the diffusive mass transfer model as a function of the Damköhler number, (41).